Advances in Applied Mathematics and Mechanics
Adv. Appl. Math. Mech., Vol. **17**, No. 1, pp. 207-223

DOI: 10.4208/aamm.OA-2023-0071
February 2025

Time-Space Adaptive Finite Element Method for Nonlinear Schrödinger Equation

Yaoyao Chen[1,*], Ying Liu[2] and Hao Wang[1]

[1] *School of Mathematics and Statistics, Anhui Normal University, Wuhu, Auhui 241000, China*
[2] *Department of Applied Mathematics, School of Science, Xi'an University of Technology, Xi'an, Shaanxi 710048, China*

Received 10 March 2023; Accepted (in revised version) 10 June 2023

Abstract. This paper is devoted to adaptive finite element method for the nonlinear Schrödinger equation. The adaptive method is based on the extrapolation technology and a second order accurate, linear and mass preserving finite element scheme. For error control, we take the difference between the numerical gradient and the recovered gradient obtained by the superconvergent cluster recovery method as the spatial discretization error estimator and the difference of numerical approximations between two consecutive time steps as the temporal discretization error estimator. A time-space adaptive algorithm is developed for numerical approximation of the nonlinear Schrödinger equation. Numerical experiments are presented to illustrate the reliability and efficiency of the proposed error estimators and the corresponding adaptive algorithm.

AMS subject classifications: 65N15, 65N30, 65N50

Key words: Nonlinear Schrödinger equation, finite element method, error estimators, time-space adaptive algorithm.

1 Introduction

In this paper, we focus on adaptive finite element method for the following nonlinear Schrödinger equation

$$iu_t+\alpha\Delta u+(v(x)+\beta|u|^2)u=0 \quad \text{in } \Omega\times(0,T], \tag{1.1}$$

subject to the initial condition

$$u(x,0)=u_0(x) \quad \text{in } \Omega\times\{0\}, \tag{1.2}$$

*Corresponding author.
Emails: cyy1012xtu@126.com (Y. Chen), wanghao106031@126.com (H. Wang), yingliu@mail.nwpu.edu.cn (Y. Liu)

and satisfies the homogeneous Dirichlet boundary condition, where Ω is a bounded open domain in R^2, $v(x)$,u denote the real-valued potential energy function and complex-valued wave function, respectively, α is the given parameter as well as β. And $i=\sqrt{-1}$ is the imaginary unit, Δ is the Laplace operator, $|\cdot|$ is the module of a complex number. It is well known that one of the important properties for equation (1.1) is the mass conservation. Computing the inner product of (1.1) with u, and taking the real parts, one can obtain the following mass conservative identity

$$\frac{d}{dt}\int_\Omega |u|^2 dx = 0. \tag{1.3}$$

The nonlinear Schrödinger equation, which was originated from quantum mechanics, is one of the most important equations in mathematical physics. It has been widely used to model various nonlinear physical phenomena, such as underwater acoustics [24], nonlinear optics [20,22], quantum condensates [11] and other nonlinear phenomena [1].

The Schrödinger equation is the most basic equation in quantum mechanics, and researchers cannot prove it from any more fundamental assumptions. Its correctness can only be tested by practice, and it is not easy to obtain the exact solution for the complex Schrödinger equation. Therefore, it is necessary to study the numerical solution of Schrödinger equation. The numerical approximations of the Schrödinger equation have been extensively investigated in the past few decades. As for the spatial discretization, it mainly includes the finite difference method [2,3,6,12], the spectral method [5], the finite element method [4,7,23,25], the discontinuous finite element method [10,19], the hybrid finite element method [18], the two grid mesh method [14,26] and references therein. And for the temporal discretization, there are Crank-Nicolson scheme [8], scalar variable auxiliary (SAV) method [9] and so on. The blow-up property of solutions is one of the important properties for the Schrödinger equation. Merle and Tsutsumi [21] proved that, for a blow-up solution with a radially symmetric initial data, the origin is a blow-up point and an L_2-concentration phenomenon occurs at the origin. In order to simulate the blow-up phenomenon described by the nonlinear Schrödinger equation, it is natural to use adaptive mesh techniques so the fine meshes are only used in a small neighborhood of the blow-up solution. The subject of a posteriori error estimates and adaptive methods for the nonlinear Schrödinger equation has been studied by some authors, we refer to [15–17] and the references therein. In [15,17], a posteriori error estimates for Crank-Nicolson finite element schemes of linear evolution Schrödinger equations were considered. T. Katsaounis and I. Kyzaa derived an optimal order a posteriori error estimates in the $L^\infty(L^2)$-norm for relaxation time discrete and fully discrete schemes of the nonlinear Schrödinger equation up to the critical exponent in [16].

In this work, we shall be interested in the numerical approximation of the blow-up solution of (1.1) with some radially symmetric initial value (1.2) in two dimensions, which is proposed by using a time-space adaptive method for the nonlinear Schrödinger equation. The adaptive method is based on the extrapolation technology and a second order accurate, linear and mass preserving finite element scheme. For the error control, we

take the difference between the numerical gradient and the recovered gradient obtained by the superconvergent cluster recovery method as the spatial discretization error estimator and the difference of numerical approximations between two consecutive time steps as the temporal discretization error estimator. In view of the proposed error estimations, a time-space adaptive algorithm is also proposed for numerical approximation of the nonlinear Schrödinger equation.

The remainder of this paper is organized as follows. In Section 2, we first give the model of nonlinear Schrödinger equation, then introduce the discrete schemes for the nonlinear Schrödinger equation. In Section 3, a posteriori error estimations, including the temporal and spatial discretization error estimators, are designed. In view of the above a posteriori error estimators, a time-space adaptive algorithm is proposed. In Section4, several numerical examples are carried out to confirm the accuracy and effectiveness of the proposed error estimators and the corresponding time-space adaptive algorithm. Finally, concluding remarks are drawn in Section 5.

2 The model and discrete scheme

For a bounded domain $\Omega \subseteq R^2$, we adopt standard notations for Sobolev spaces such as $W^{m,p}(\Omega)$ equipped with the norm $\|\cdot\|_{m,p,\Omega}$ and semi-norm $|\cdot|_{m,p,\Omega}$. If $p=2$, we set $W^{m,p}(\Omega)=H^m(\Omega)$, $\|\cdot\|_{m,p,\Omega}=\|\cdot\|_{m,\Omega}$ and $|\cdot|_{m,p,\Omega}=|\cdot|_{m,\Omega}$. We also denote $\|v\|=\|v\|_{0,\Omega}$ and take $\partial\Omega$ as the boundary of Ω.

2.1 The model problem

Let $u=p+iq$, then Eqs. (1.1)-(1.2) can be rewritten as the following real-value equations

$$\begin{cases} p_t+\alpha\Delta q+Bq=0 & \text{in } \Omega\times(0,T], \\ q_t-\alpha\Delta p-Bp=0 & \text{in } \Omega\times(0,T], \\ p=p_0, \quad q=q_0 & \text{in } \Omega\times\{0\}, \\ p=0, \quad q=0 & \text{on } \partial\Omega\times(0,T], \end{cases} \tag{2.1}$$

with $B=v(x)+\beta|u|^2$, $|u|^2=p^2+q^2$.

The weak form of Eq. (2.1) is as follows: find $(p,q)\in C_0([0,T],H_0^1(\Omega))$ such that

$$\begin{cases} (p_t,\phi)-(\alpha\nabla q,\nabla\phi)+(Bq,\phi)=0, & \forall\phi\in H_0^1(\Omega), \\ (q_t,\varphi)+(\alpha\nabla p,\nabla\varphi)-(Bp,\varphi)=0, & \forall\varphi\in H_0^1(\Omega). \end{cases} \tag{2.2}$$

2.2 The semi-discrete scheme

Let $\mathcal{T}_h$ be a shape regular triangulation of Ω and V_h be the corresponding finite element space, which is defined as

$$V_h=\{w\in C(\bar{\Omega}):w|_K\in P^k(K),\ K\in\mathcal{T}_h,\ w=0 \text{ on } \partial\Omega\},$$

where $C(\bar{\Omega})$ is the continuous functional space and $P^k(K)$ denotes the space of polynomials of degree no more than k defined in $K\subseteq R^2$.

The semi-discrete finite element scheme of (2.1) reads: find $(p_h,q_h)\in V_h\times V_h$ such that

$$\begin{cases} ((p_h)_t,\phi_h)-(\alpha\nabla q_h,\nabla\phi_h)+(B_hq_h,\phi_h)=0, & \forall\phi_h\in V_h,\\ ((q_h)_t,\varphi_h)+(\alpha\nabla p_h,\nabla\varphi_h)-(B_hp_h,\varphi_h)=0, & \forall\varphi_h\in V_h,\\ p_h(x,0)=\Pi_hp_0, \quad q_h(x,0)=\Pi_hq_0, \end{cases} \tag{2.3}$$

where $B_h=v(x)+\beta|u_h|^2$ and Π_h denotes the L^2-projection, i.e., for each $w\in L^2(\Omega)$, it holds that

$$(\Pi_hw,\phi_h)=(w,\phi_h), \quad \forall\phi_h\in V_h.$$

Theorem 2.1. *For the nonlinear Schrödinger equation* (2.1)*, the semi-discrete numerical solutions of* (p,q) *satisfy the following mass conservation law*

$$\frac{d}{2dt}\left(\|p_h\|^2+\|q_h\|^2\right)=0, \tag{2.4}$$

and energy conservation law

$$\begin{aligned}\frac{d}{dt}\Bigg(&\frac{\alpha}{2}\left(\|\nabla p_h\|^2+\|\nabla q_h\|^2\right)-\frac{v(x)}{2}\left(\|p_h\|^2+\|q_h\|^2\right)\\ &-\frac{\beta}{4}\left(\|p_h\|^4+\|q_h\|^4+2\|p_h\|^2\|q_h\|^2\right)\Bigg)=0.\end{aligned} \tag{2.5}$$

Proof. On the one hand, let $\phi_h=p_h,\varphi_h=q_h$ in (2.3), it holds that

$$\begin{cases} ((p_h)_t,p_h)-(\alpha\nabla q_h,\nabla p_h)+(B_hq_h,p_h)=0,\\ ((q_h)_t,q_h)+(\alpha\nabla p_h,\nabla q_h)-(B_hp_h,q_h)=0. \end{cases} \tag{2.6}$$

Adding the above two equations together, we obtain

$$\frac{d}{2dt}\left(\|p_h\|^2+\|q_h\|^2\right)=0.$$

On the other hand, we take the test function as $\phi_h=(q_h)_t$, $\varphi_h=(p_h)_t$ in (2.3), then it gets

$$\begin{cases} ((p_h)_t,(q_h)_t)-(\alpha\nabla q_h,\nabla(q_h)_t)+(B_hq_h,(q_h)_t)=0,\\ ((q_h)_t,(p_h)_t)+(\alpha\nabla p_h,\nabla(p_h)_t)-(B_hp_h,(p_h)_t)=0. \end{cases} \tag{2.7}$$

Let the second equation minus the first equation in (2.7), we have

$$(\alpha\nabla p_h,\nabla(p_h)_t)+(\alpha\nabla q_h,\nabla(q_h)_t)-(B_hp_h,(p_h)_t)-(B_hq_h,(q_h)_t)=0. \tag{2.8}$$

Further, we have

$$\frac{\alpha}{2}\frac{d}{dt}\left(\|\nabla p_h\|^2+\|\nabla q_h\|^2\right)-\frac{v(x)}{2}\frac{d}{dt}\left(\|p_h\|^2+\|q_h\|^2\right)$$
$$-\frac{\beta}{4}\frac{d}{dt}\left(\|p_h\|^4+\|q_h\|^4+2\|p_h\|^2\|q_h\|^2\right)=0.$$

This completes the proof. □

2.3 The fully discrete scheme

We subdivide the time interval $[0,T]$ into a partition of N consecutive adjacent subintervals whose endpoints are denoted by $0=t_0<t_1<\cdots<t_N=T$, the n-th time interval $I_n:=[t_{n-1},t_n]$, the corresponding time step and finite element space are defined as $\tau_n:=t_n-t_{n-1}$ and V_h^n, respectively. The fully discrete finite element scheme of (2.1) reads: find a sequence of function $(p_h^{n+1},q_h^{n+1})\in V_h^{n+1}\times V_h^{n+1}$ such that, for each $n=1,2,\cdots,N$, it holds

$$\begin{cases}(D_t p_h^{n+1},\phi_h)-(\alpha\nabla q_h^{n+\frac{1}{2}},\nabla\phi_h)+(\Pi_h^{n+1}\tilde{B}_h^n q_h^{n+\frac{1}{2}},\phi_h)=0,\\ (D_t q_h^{n+1},\varphi_h)+(\alpha\nabla p_h^{n+\frac{1}{2}},\nabla\varphi_h)-(\Pi_h^{n+1}\tilde{B}_h^n p_h^{n+\frac{1}{2}},\varphi_h)=0,\end{cases}\tag{2.9}$$

where

$$p_h^{n+\frac{1}{2}}=\frac{p_h^{n+1}+\Pi_h^{n+1}p_h^n}{2},\qquad D_t p_h^{n+1}=\frac{p_h^{n+1}-\Pi_h^{n+1}p_h^n}{\tau_{n+1}},\tag{2.10a}$$
$$q_h^{n+\frac{1}{2}}=\frac{q_h^{n+1}+\Pi_h^{n+1}q_h^n}{2},\qquad D_t q_h^{n+1}=\frac{q_h^{n+1}-\Pi_h^{n+1}q_h^n}{\tau_{n+1}},\tag{2.10b}$$

and

$$\tilde{B}_h^n=\frac{3B_h^n-\Pi_h^n B_h^{n-1}}{2},\quad B_h^n=(v(x)+\beta|u_h^n|^2),\quad |u_h^n|^2=(p_h^n)^2+(q_h^n)^2,\tag{2.11}$$

with Π_h^n being the Lagrange interpolation operator of V_h^{n-1} to V_h^n.

Remark 2.1. Note that this scheme is a three-level scheme in which we need the approximations (p_h^n,q_h^n) and (p_h^{n-1},q_h^{n-1}) to obtain the numerical solution (p_h^{n+1},q_h^{n+1}) at time t_{n+1}. In our numerical examples, we apply the backward Euler scheme to obtain (p_h^1,q_h^1) at time t_1, then we use (2.9) to obtain numerical solution (p_h^{n+1},q_h^{n+1}), $n=1,2,3,\cdots,N$ at the other time steps.

Theorem 2.2. *For the nonlinear Schrödinger equation* (2.1)*, the fully discrete numerical solutions of* (p,q) *satisfy the following modified mass conservation law*

$$\int (p_h^{n+1})^2+(q_h^{n+1})^2dx=\int(\Pi_h^{n+1}p_h^n)^2+(\Pi_h^{n+1}q_h^n)^2dx.\tag{2.12}$$

Proof. Taking the test function as

$$\phi_h = p_h^{n+1} - \Pi_h^{n+1} p_h^n, \quad \varphi_h = q_h^{n+1} - \Pi_h^{n+1} q_h^n$$

in (2.9), we obtain

$$\begin{cases} \left(\dfrac{p_h^{n+1} - \Pi_h^{n+1} p_h^n}{\tau_{n+1}}, p_h^{n+1} - \Pi_h^{n+1} p_h^n \right) - \left(\alpha \nabla q_h^{n+\frac{1}{2}}, \nabla (p_h^{n+1} - \Pi_h^{n+1} p_h^n) \right) \\ \quad + \left(\Pi_h^{n+1} \tilde{B}_h^n q_h^{n+\frac{1}{2}}, p_h^{n+1} - \Pi_h^{n+1} p_h^n \right) = 0, \\ \left(\dfrac{q_h^{n+1} - \Pi_h^{n+1} q_h^n}{\tau_{n+1}}, q_h^{n+1} - \Pi_h^{n+1} q_h^n \right) + \left(\alpha \nabla p_h^{n+\frac{1}{2}}, \nabla (q_h^{n+1} - \Pi_h^{n+1} q_h^n) \right) \\ \quad - \left(\Pi_h^{n+1} \tilde{B}_h^n p_h^{n+\frac{1}{2}}, q_h^{n+1} - \Pi_h^{n+1} q_h^n \right) = 0. \end{cases} \tag{2.13}$$

Then adding the above two equations together, we have

$$\|p_h^{n+1}\|^2 + \|q_h^{n+1}\|^2 - \|\Pi_h^{n+1} p_h^n\|^2 - \|\Pi_h^{n+1} q_h^n\|^2 = 0. \tag{2.14}$$

Thus the law of modified mass conservation is proved. □

3 A posteriori error estimations and adaptive algorithm

In this section, the recovery type a posteriori error estimation for spatial discretization and an error indicator for time adaptation of the nonlinear Schrödinger equation are introduced. And a time-space adaptive algorithm is designed based on the proposed error indicators.

3.1 A posteriori error estimation

Let $R_h : V_h \to V_h \times V_h$ be the superconvergent cluster recovery (SCR) operator. As for the SCR method, we first need to define the recovered gradient at the vertex nodes, after determining values of the recovery gradient at all nodes, we obtain it on the whole domain by interpolation using the original nodal shape functions of the finite element space, which the detail procedure is shown in Algorithm 3.1.

Remark 3.1. As for the SCR method, the symmetry of sample points play an important role for improving the accuracy of the SCR-recovered gradient. In general, we can use the following three different ways to sampling the points, which are shown in Fig. 1. In Case 1, we set all the mesh nodes as the sampling points, while in Case 2 and Case 3, we select four points which are symmetric with respect to the recovering point. The SCR can improve the approximation order while the sampling points are mesh nodes and symmetrically around the recovering point. And if the sampling points are symmetrical but not the mesh nodes, it can improve the accuracy of the SCR-recovered gradient.

Algorithm 3.1 The SCR algorithm.

1: For a given mesh $\mathcal{T}_h$ and a finite element approximation u_h, the SCR method processes the following two steps to obtain the recovered gradient $R_h u_h$.

2: Step 1: Define the SCR-recovered gradient at $z \in \mathcal{N}_h$.

- For an interior vertex $z \in \mathcal{N}_h \cap \Omega$, we select some points $z_i = (x_i, y_i), 1 \le i \le n$ (at least 4) so that they locate around z as symmetrically as possible. Generally, choosing the mesh nodes performs well. Let $\mathcal{K}_z$ denote the convex polygon of the sampling points. We find a linear polynomial satisfying

$$p_z(x,y) := arg \min_{p_1 \in P_1} \sum_{i=1}^{n} (p_1(z_i) - u_h(z_i))^2, \tag{3.1}$$

  and the recovered gradient at z is defined by

$$R_h u_h(z) = \nabla p_z(x_z, y_z). \tag{3.2}$$

- If $z \in \partial\Omega$ and no internal mesh node is directly connected to it, the recovered gradient at z is defined to be $R_h u_h(z) = \nabla u_h(z)$.

- If $z \in \partial\Omega$ and there are some internal mesh nodes $z_1, z_2, \cdots, z_{N_z}$ directly connected to it, we first obtain the linear polynomial $p_{z_i}(x,y)$ which is best to fit u_h at the sampling points of $\mathcal{K}_{z_i}$ for each internal mesh nodes z_i, $i = 1,2,\ldots,N_z$, then the recovered gradient at z is defined to be

$$R_h u_h(z) = \frac{1}{N_z} \sum_{i=1}^{N_z} \nabla p_{z_i}(z).$$

3: Step 2: The recovered gradient $R_h u_h$ on Ω is obtained by the interpolation

$$R_h u_h = \sum_{z \in \mathcal{N}_h} (R_h u_h)(z) \phi_z, \tag{3.3}$$

where ϕ_z is the Lagrange basis of V_h on node z.

Remark 3.2. The SCR method is a post-processing technique that reconstructs improved gradient approximations from finite element solutions, which not only can improve the quality of the approximation, but also construct a posteriori error estimators in adaptive computation. And the SCR-based estimators have gained widely applications in engineering practice.

In view of the SCR recovery operator, we define the following SCR-based error esti-

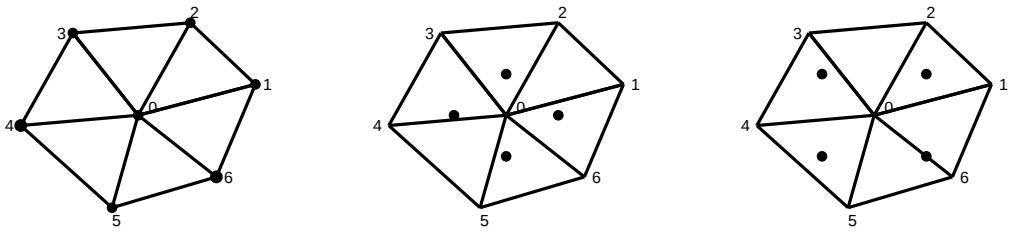

Case 1 Case 2 Case 3

Figure 1: • sampling points [13].

mator for the spatial adaptation

$$\eta_{K,p} = \|R_h p_h - \nabla p_h\|_{0,K}, \quad \eta_{K,q} = \|R_h q_h - \nabla q_h\|_{0,K}, \tag{3.4a}$$

$$\eta^2 = \frac{\sum_{K\in\mathcal{T}_h}(\eta_{K,p}^2 + \eta_{K,q}^2)}{NT}, \tag{3.4b}$$

where $\eta_{K,p}$, $\eta_{K,q}$ are denoted as the local error indicators of real and imaginary parts, respectively, η is the global error estimator.

As for the temporal adaptation, the variable time steps are used and the difference of the numerical approximations between two time steps

$$\eta_k^{n+1} := \|u_h^{n+1} - \Pi_h^{n+1} u_h^n\|$$

is chosen as the temporal discretization error estimator.

3.2 Adaptive algorithm

In view of the error indicators above, we design the following time-space adaptive algorithm for the nonlinear Schrödinger equation, which is outlined in Algorithm 3.2. And in the Marking procedure, the maximum strategy is used for marking the elements for refinement or coarsening as shown in Algorithm 3.3.

4 Numerical examples

In this section, several numerical examples are given to demonstrate the reliability and effectiveness of the proposed numerical scheme and adaptive algorithm for the nonlinear Schrödinger equation.

4.1 Tests for the rate of convergence

In this part, the convergent rates of time and space for the nonlinear Schrödinger equation are given in Example 4.1, respectively. And the mass conservation law is also verified.

Algorithm 3.2 Time-space adaptive algorithm for the nonlinear Schrödinger equation.

Given $TOL_t, TOL_{t,\min}, TOL_s, TOL_e$, $\delta_1 \in (0,1)$, $\delta_2 > 1$;
Start with initial time step τ_0, initial mesh $\mathcal{T}_h^0$, and initial solution (p_h^0, q_h^0);
Set $n=0$, $t_0=0$ and compute the energy $E(u_h^0)$;
Set $\mathcal{T}_h^1 := \mathcal{T}_h^0, \tau_1 := \tau_0$ and $t_1 = t_0 + \tau_1$;
Solve the discrete equation for (p_h^1, q_h^1) on mesh $\mathcal{T}_h^1$ by using backward Euler method;
Do time and space adaptation and compute the energy $E(u_h^1)$;
while $E(u_h^n) - E(u_h^{n-1}) > TOL_e$ **do**
  Set $\mathcal{T}_h^{n+1} := \mathcal{T}_h^n, \tau_{n+1} := \tau_n$ and $t_{n+1} = t_n + \tau_{n+1}$;
  Solve the discrete equation for (p_h^{n+1}, q_h^{n+1}) on mesh $\mathcal{T}_h^{n+1}$ using data (p_h^n, q_h^n);
  Compute the time error estimator η_k^{n+1};
  while $\eta_k^{n+1} > TOL_t$ or $\eta_k^{n+1} < TOL_{t,\min}$ **do**
    if $\eta_k^{n+1} > TOL_t$ **then**
      Set $\tau_{n+1} := \delta_1 \cdot \tau_{n+1}$ and $t_{n+1} = t_n + \tau_{n+1}$;
    else
      Set $\tau_{n+1} := \delta_2 \cdot \tau_{n+1}$ and $t_{n+1} = t_n + \tau_{n+1}$;
    end if
    Solve the discrete equation for (p_h^{n+1}, q_h^{n+1}) on mesh $\mathcal{T}_h^{n+1}$ using data (p_h^n, q_h^n);
    Compute the time error estimator η_k^{n+1};
  end while
  Compute the space error estimator $\{\eta_{K,p}^{n+1}\}, \{\eta_{K,q}^{n+1}\}, \eta^{n+1}$;
  while $\eta_h^{n+1} > TOL_s$ **do**
    Mark elements for refinement or coarsening;
    Refine and coarsen mesh $\mathcal{T}_h^{n+1}$ to generate a new mesh $\mathcal{T}_h^{n+1}$;
    Solve the discrete equation for (p_h^{n+1}, q_h^{n+1}) on mesh $\mathcal{T}_h^{n+1}$ using data (p_h^n, q_h^n);
    Compute the error estimators η_k^{n+1};
    while $\eta_k^{n+1} > TOL_{time}$ or $\eta_k^{n+1} < TOL_{t,min}$ **do**
      if $\eta_k^{n+1} > TOL_{time}$ **then**
        Set $\tau_{n+1} := \delta_1 \cdot \tau_{n+1}$ and $t_{n+1} = t_n + \tau_{n+1}$;
      else
        Set $\tau_{n+1} := \delta_2 \cdot \tau_{n+1}$ and $t_{n+1} = t_n + \tau_{n+1}$;
      end if
      Solve the discrete equation for (p_h^{n+1}, q_h^{n+1}) on mesh $\mathcal{T}_h^{n+1}$ using data (p_h^n, q_h^n);
      Compute the error estimators η_k^{n+1};
    end while
    Compute the error estimators $\{\eta_{K,p}^{n+1}\}, \{\eta_{K,q}^{n+1}\}, \eta^{n+1}$;
  end while
  Compute the energy $E(u_h^{n+1})$;
  $n = n+1$;
end while

Example 4.1 ([27]). In the first example, let $\bar{\Omega} = [0,\pi]^2$ and the parameters $\alpha = 1$, $\beta = 1$, $v(x) = -\sin^2 x \sin^2 y$, we consider the nonlinear Schrödinger equation (1.1) with the exact

Algorithm 3.3 Marking strategy.

1: Given the element error estimators $\{\eta_{K,p}^{n+1}\}$, $\{\eta_{K,q}^{n+1}\}$ on mesh $\mathcal{T}_{n+1}^h$ and two parameters:
$$\theta_r \in \left(\frac{1}{2},1\right), \qquad \theta_c \in \left(0,\frac{1}{2}\right).$$
2: Output two element sets:
$$\mathcal{M}_r = \{K : \eta_{K,p}^{n+1} > \theta_r \eta_{\max,p}^{n+1} \text{ or } \eta_{K,q}^{n+1} > \theta_r \eta_{\max,q}^{n+1}, K \in \mathcal{T}_h^{n+1}\},$$
$$\mathcal{M}_c = \{K : \eta_{K,p}^{n+1} < \theta_c \eta_{\max,p}^{n+1} \text{ and } \eta_{K,q}^{n+1} < \theta_c \eta_{\max,q}^{n+1}, K \in \mathcal{T}_h^{n+1}\}.$$
3: Calculate the maximum element error estimators:
$$\eta_{\max,p}^{n+1} := \max\{\eta_{K,p}^{n+1}, K \in \mathcal{T}_h^{n+1}\},$$
$$\eta_{\max,q}^{n+1} := \max\{\eta_{K,q}^{n+1}, K \in \mathcal{T}_h^{n+1}\}.$$
4: **for all** $K \in \mathcal{T}_h^{n+1}$ **do**
5: **if** $\eta_{K,p}^{n+1} > \theta_r \eta_{\max,p}^{n+1}$ or $\eta_{K,q}^{n+1} > \theta_r \eta_{\max,q}^{n+1}$ **then**
6: $\mathcal{M}_r = \mathcal{M}_r + \{K\}$;
7: **else** $\eta_{K,p}^{n+1} < \theta_c \eta_{\max,p}^{n+1}$ and $\eta_{K,q}^{n+1} < \theta_c \eta_{\max,q}^{n+1}$
8: $\mathcal{M}_c = \mathcal{M}_c + \{K\}$;
9: **end if**

solution
$$u = e^{-2it} \sin x \sin y.$$

The spatial and temporal convergent rates of the proposed methods for the nonlinear Schrödinger equation are shown in Tables 1-2, respectively. From the tables, we can see that the spatial accuracy is $k+1$ order for the L_2 norm, and it is k order for the H_1 norm. As for the temporal accuracy, it is second order.

In order to verify the mass conservation law, we plot the picture of mass in Fig. 2. As it is shown that the mass is conserved, which is matched with the Theorem 3.1.

4.2 Numerical simulations for adaptive method

In order to verify the reliability and effectiveness of the proposed adaptive algorithm, in this part, we solve the nonlinear Schrödinger equation based on the designed adaptive algorithm.

Example 4.2 ([27]). Given a circular area $x^2+y^2 \leq 5$, consider the nonlinear Schrödinger equation (1.1) with the initial condition
$$u_0(x,y) = 6\sqrt{2}e^{-(x^2+y^2)},$$

Table 1: Example 4.1, L_2 error and convergent rate of space, $T=0.5$.

k	τ_{n+1}	m	L_2-error	Order	H_1-error	Order
1	1e-03	5	2.1407e-01	-	7.2800e-01	-
	1e-03	10	5.6431e-02	1.9235	3.5351e-01	1.0422
	1e-03	20	1.4290e-02	1.9815	1.7507e-01	1.0138
	1e-03	40	3.5789e-03	1.9974	8.7311e-02	1.0037
2	1e-03	5	7.3176e-03	-	8.5194e-02	-
	1e-03	10	9.0298e-04	3.0186	2.1532e-02	1.9843
	1e-03	20	1.1102e-04	3.0238	5.3981e-03	1.9959
	1e-03	40	1.3851e-05	3.0028	1.3508e-03	1.9987
3	2.5e-04	5	5.5912e-04	-	7.8476e-03	-
	2.5e-04	10	3.4379e-05	3.9815	9.8703e-04	2.9911
	2.5e-04	20	2.0541e-06	4.0649	1.2181e-04	3.0185
	2.5e-04	40	1.3348e-07	3.9894	1.5120e-05	3.0101

Table 2: Example 4.1, L_2 error and convergent rate of time (P^3 element, the size of mesh $\frac{\pi}{40}\times\frac{\pi}{40}$).

τ_{n+1}	L_2 error	Order
0.1	4.1638e-03	-
0.05	1.1763e-03	1.8236
0.025	3.1075e-04	1.9204
0.0125	7.9742e-05	1.9624

and the parameters $\alpha=1$, $\beta=1$, $v(x)=0$.

Fig. 3 shows the initial mesh and the contour plot of initial function u_0, which incloses a cone shape. The sequence of adaptive meshes and the snapshots of the corresponding approximate solutions are displayed in Fig. 4. From the numerical result, we can see

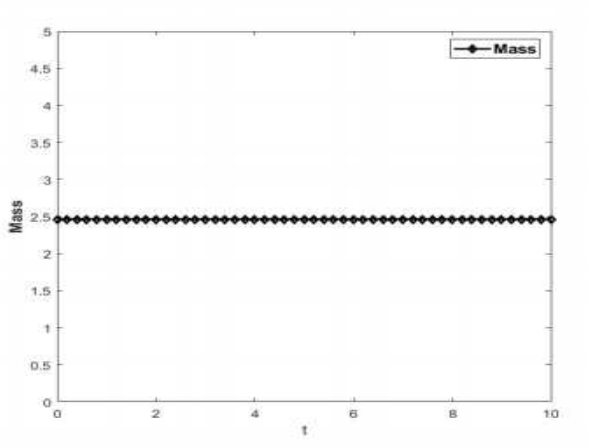

Figure 2: Example 4.1, snapshot of mass.

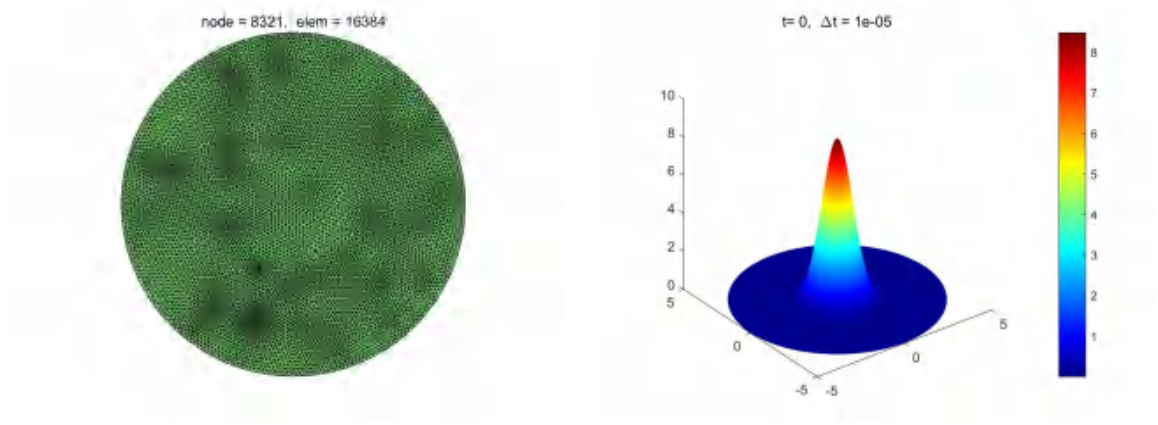

(a) (b)

Figure 3: Example 4.2, snapshots of initial mesh and initial solution.

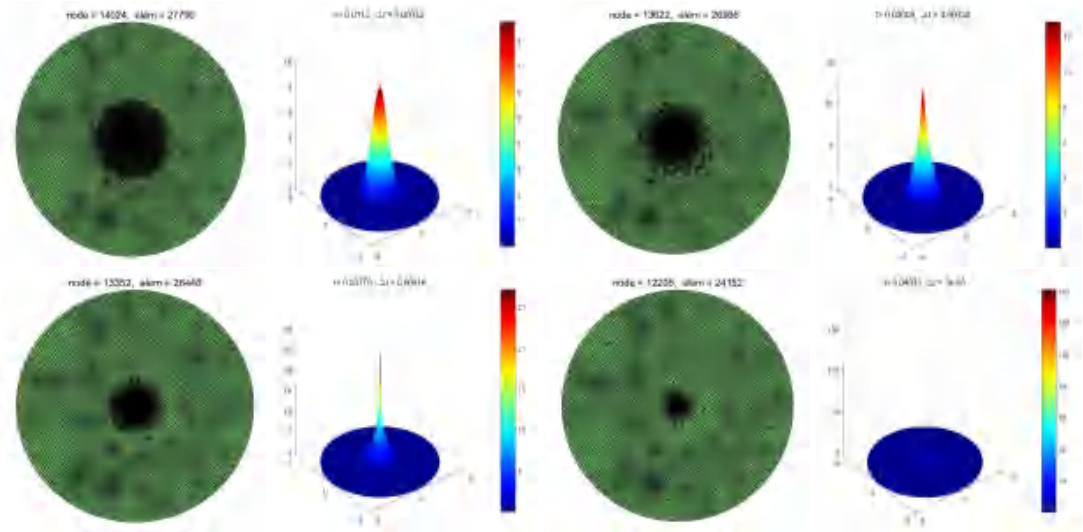

Figure 4: Example 4.2, snapshots of adaptive meshes and numerical solutions.

that the blow-up phenomenon and mesh refinement near the blow-up solutions, and the number of nodes becomes smaller and smaller as the zeros level curve becomes shorter and shorter.

In Fig. 5, the contour plot of the change of number for nodes and time-steps with time for the nonlinear Schrödinger equation based on the proposed time-space adaptive algorithm are displayed. From the pictures, we can see clearly that the number of nodes decreases over time and the time-steps are changed with time. Further, in order to show the efficiency of the proposed time-space adaptive algorithm, we solve nonlinear

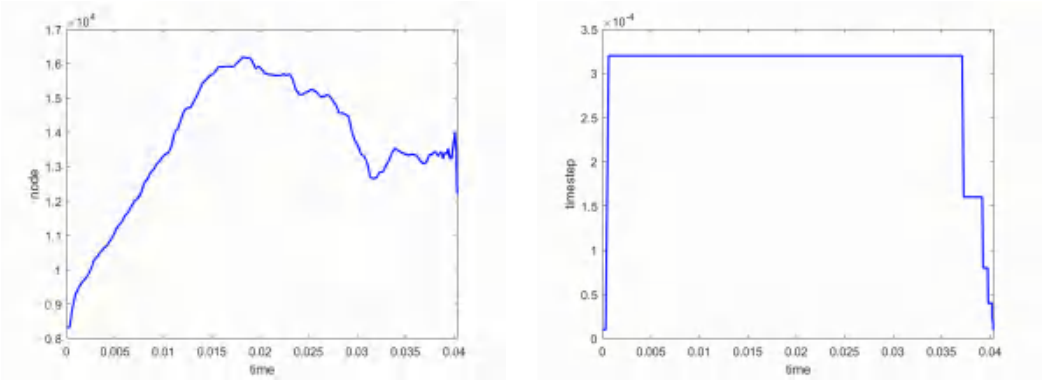

(a) (b)

Figure 5: Example 4.2, (a) number of nodes; (b) time-steps.

Schrödinger equation based on Algorithm 3.2 and only space adaptation, respectively, for which the initial time-steps are both taken as $1e-5$. The CPU time based on the two kinds of adaptive algorithms are given in Table 3 for Example 4.2. As it is shown, we can see that the CPU time in view of the only space adaptation is more than five times that of the time-space adaptive algorithm, which indicates that the proposed time-space adaptive algorithm is more efficient.

Table 3: Example 4.2 $(T=0.04)$, CPU time of two kinds of algorithms (11th Gen Intel(R) Core(TM) i5-1135G7 @ 2.40GHz 2.42GHz).

Algorithms	Time-space adaptive algorithm	Space adaptive algorithm
CPU time	706s	174478s

Example 4.3 ([27])**.** In the last example, we consider the nonlinear Schrödinger equation

$$\begin{cases} iu_t+\alpha\Delta u+(v(x)+\beta|u|^2)u=f & \text{in } \Omega\times(0,T], \\ u(x,0)=u_0(x) & \text{in } \Omega\times\{0\}, \\ u=0 & \text{on } \partial\Omega\times(0,T], \end{cases} \tag{4.1}$$

with the following exact solution

$$u=\frac{e^t\sin(\pi x)\sin(\pi y)}{(x+0.5)^2+(y-0.5)^2+0.01}+i\frac{e^t\sin(\pi x)\sin(\pi y)}{(x-0.5)^2+(y+0.5)^2+0.01},$$

where $\bar{\Omega}=[-1,1]^2$, $\alpha=\frac{1}{2}$, $\beta=1$, $v(x)=0$, and the corresponding right term f can be obtained by taking u into Eq. (4.1).

Fig. 6 displays initial mesh and the contour plot of the initial solution u_0, which incloses cone type with symmetry. We present the sequence of adaptive meshes and con-

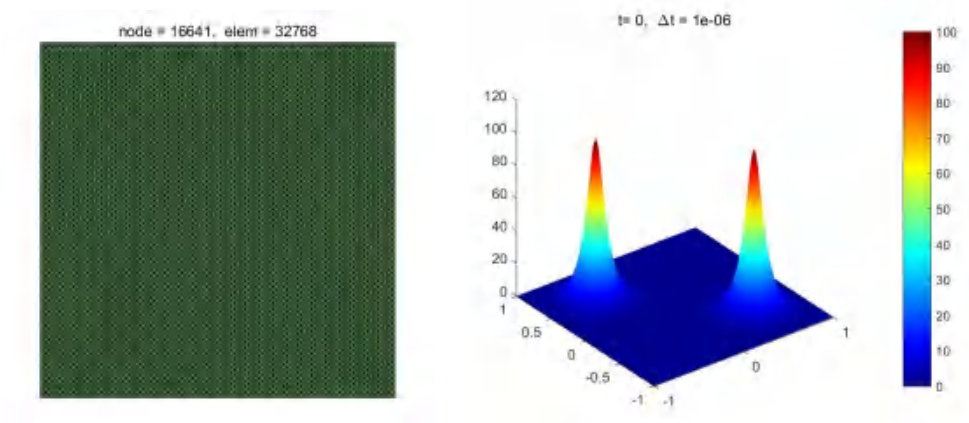

Figure 6: Example 4.3, snapshots of initial mesh and initial solution.

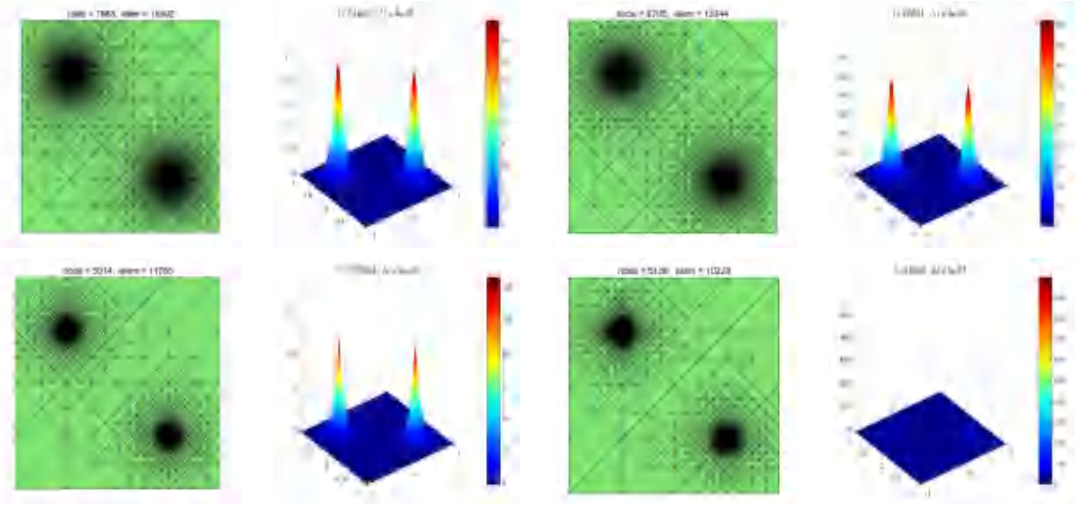

Figure 7: Example 4.3, snapshots of adaptive meshes and numerical solutions.

tour plots of the corresponding approximate solutions produced by the adaptive algorithm in Fig. 7. The initially connected interface splits into two curves, then the two component of the interface develop circular shapes and the diameters of the two particles decrease to zero until they collapse. Once again, it clearly shows the fine mesh follows the zeros level set as it moves, and the number of nodes becomes smaller and smaller as the zeros level curve becomes shorter and shorter.

The snapshots of the number of nodes and time-steps by using the proposed time-space adaptive algorithm for Example 4.3 are shown in Fig. 8. And in order to compare the proposed time-space adaptive algorithm with the spatial adaptation, the initial time-

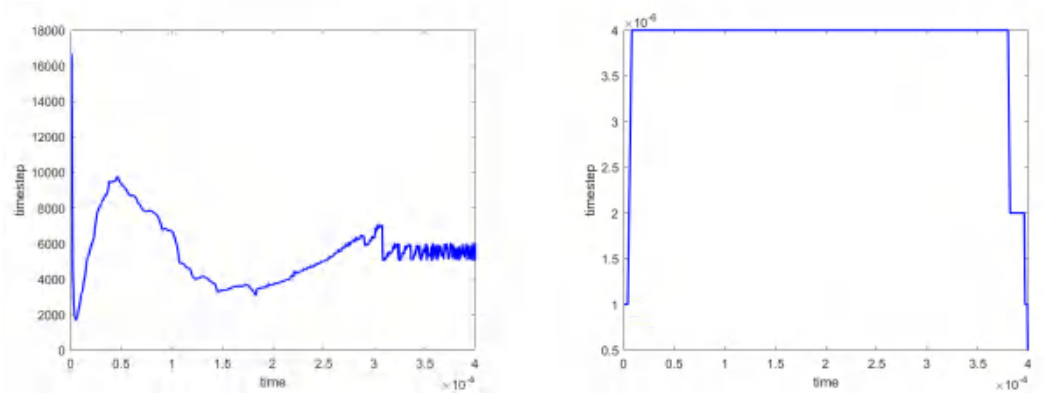

(a) (b)

Figure 8: Example 4.3, (a) number of nodes; (b) time-steps.

steps is given as $1e$-6. The according CPU time based on the two kinds of adaptive algorithms are given in Table 4. Once again, we can see that clearly that the number of nodes decreases over time and the CPU time of the proposed time-space adaptive algorithm is more shorter.

Table 4: Example 4.3 $(T=4e-4)$, CPU time of two kinds of algorithms (11th Gen Intel(R) Core(TM) i5-1135G7 @ 2.40GHz 2.42GHz).

Algorithms	Time-space adaptive algorithm	Space adaptive algorithm
CPU time	3306s	4553s

5 Conclusions

In this paper, we considered the adaptive finite element method for the nonlinear Schrödinger equation. The adaptive method was based on a second order accurate finite element scheme and a recovery-type a posteriori error estimator. A SCR-based a posteriori error estimation was derived to control the mesh refinement and coarsening. In view of the proposed error indicators, a time-space adaptive algorithm was proposed for numerical approximation of the nonlinear Schrödinger equation. Numerical experiments were presented to illustrate the reliability and efficiency of the proposed error estimators and the corresponding adaptive algorithm.

Acknowledgements

Chen's research was partially supported by NSFC Project (No. 12201010), Natural Science Research Project of Higher Education in Anhui Province (No. 2022AH040027), the

Scientific Research Foundation for Scholars of Anhui Normal University (No. 762135) and the Research Culture Funds of Anhui Normal University (No. 2022xjxm035). Wang's research was partially supported by Natural Science Research Project of Higher Education in Anhui Province (No. 2022AH050205) and the Scientific Research Foundation for Scholars of Anhui Normal University (No. 762133).

References

[1] M. Ablowitz and H. Segue, Solitons and the Inverse Scattering Transformation, SIAM, Philadelphia, 1981.
[2] G. D. Akrivis, *Finite difference discretization of the cubic Schrödinger equations,* IMA J. Numer. Anal., 13(1) (1993), pp. 115–124.
[3] X. Antoine, W. Bao and C. Besse, *Computational methods for the dynamics of the nonlinear Schrödinger/Gross-Pitaevskii equations,* Comput. Phys. Commun., 184(12) (2013), pp. 2621–2633.
[4] D. C. Antonopoulou, G. D. Karali, M. Plexousakis and G. E. Zouraris, *Crank-Nicolson finite element discretizations for a two-dimensional linear Schrödinger-type equation posed in a noncylindrical domain,* Math. Comput., 84(294) (2015), pp. 1571–1598.
[5] W. Bao and Y. Cai, *Uniform and optimal error estimates of an exponential wave integrator sine pseudospectral method for the nonlinear Schrödinger equation with wave operator,* SIAM J. Numer. Anal., 52(3) (2014), pp. 1103–1127.
[6] W. Bao and Y. Cai, *Uniform error estimates of finite difference methods for the nonlinear Schrödinger equation with wave operator,* SIAM J. Numer. Anal., 50(2) (2012), pp. 492–521.
[7] W. Cai, D. He and K. Pan, *A linearized energy-conservative finite element method for the nonlinear Schrödinger equation with wave operator,* Appl. Numer. Math., 140 (2019), pp. 183–198.
[8] M. Delfour, M. Fortin and G. Payr, *Finite-difference solutions of a non-linear Schrödinger equation,* J. Comput. Phys., 44(2) (1981), pp. 277–288.
[9] X. Feng, B. Li and S. Ma, *High-order mass-and energy-conserving SAV-Gauss collocation finite element methods for the nonlinear Schrödinger equation,* SIAM J. Numer. Anal., 59(3) (2021), pp. 1566–1591.
[10] L. Guo and Y. Xu, *Energy conserving local discontinuous Galerkin methods for the nonlinear Schrödinger equations with wave operator,* J. Sci. Comput., 65(2) (2015), pp. 622–647.
[11] A. Hasegawa and Y. Kodama, Solitons in Optical Communications, Oxford University Press, New York, 1995.
[12] X. Hu and L. Zhang, *Conservative compact difference schemes for the coupled nonlinear Schrödinger system,* Numer. Meth. Part. D. E., 30(3) (2014), pp. 749–772.
[13] Y. Huang and N. Yi, *The superconvergent cluster recovery method,* J. Sci. Comput., 44 (2010), pp. 301–322.
[14] J. Jin, N. Wei and H. Zhang, *A two-grid finite-element method for the nonlinear Schrödinger equation,* J. Comput. Math., 33(2) (2015), pp. 146–157.
[15] T. Katsaounis and I. Kyza, *A posteriori error control and adaptivity for Crank-Nicolson finite element approximations for the linear Schrödinger equation,* Numer. Math., 129 (2015), pp. 55–90.
[16] T. Katsaounis and I. Kyza, *A posteriori error analysis for evolution nonlinear Schrödinger equations up to the critical exponent,* SIAM J. Numer. Anal., 56(3) (2016), pp. 1–23.
[17] I. Kyza, *A posteriori error analysis for the Crank-Nicolson method for linear Schrödinger equations,* ESAIM Math. Model. Numer. Anal., 45 (2011), pp. 761–778.

[18] Y. LIU AND H. LI, *H^1-Galerkin mixed finite element method for the linear Schrödinger equation,* Adv. Math., 39(4) (2010), pp. 429–442.
[19] W. LU, Y. HUANG AND H. LIU, *Mass preserving discontinuous Galerkin methods for Schrödinger equations,* J. Comput. Phys., 282 (2015), pp. 210–226.
[20] B. MALOMED, Nonlinear Schrödinger Equation with Wave Operator, in: Alwyn Scot (Ed.), Encyclopedia of Nonlinear Science, Routledge, New York, 2005.
[21] F. MERLE AND Y. TSUTSUMI, *L2-concentration of blow-up solutions for the nonlinear Schrödinger equation with critical power nonlinearity,* J. Differ. Equations, 84 (1990), pp. 205–214.
[22] A. NEWELL, Solitons in Mathematics and Physics, SIAM, Philadelphia, 1985.
[23] Y. SUI, D. ZHANG, J. CAO AND J. ZHANG, *An efficient finite element method and error analysis for eigenvalue problem of Schrödinger equation with an inverse square potential on spherical domain,* Adv. Differ. Equ., 582 (2020).
[24] F. TAPPERT, The Parabolic Approximation Method, in: J. B. Keller, J. S. Papadaskis (Eds.). Wave Propagation and Underwater Acoustics, in: Lect. Notes Phys., Springer, Berlin, 70 (1977), pp. 224–287.
[25] J. WANG, M. LI AND Y. ZHANG, *Superconvergence analysis of BDF-Galerkin FEM for nonlinear Schrödinger equation,* Numer. Algorithms, 89 (2022), pp. 1–28..
[26] H. ZHANG, J. JIN AND J. WANG, *Two-grid finite-element method for the two-dimensional time-dependent Schrödinger equation,* Adv. Appl. Math. Mech., 5(2) (2013), pp. 180–193.
[27] R. ZHANG, X. YU, M. LI AND ET AL., *A conservative local discontinuous Galerkin method for the solution of nonlinear Schrödinger equation in two dimensions,* Sci. China Math., 60 (2017), pp. 2515–2530.